PROCEEDINGS OF SCIENCE

Studies on finite-volume effects in the inclusive semileptonic decays of charmed mesons

Ryan Kellermann,[a,*] **Alessandro Barone,**[b,c,d] **Shoji Hashimoto,**[a] **Andreas Jüttner**[c,d,e] **and Takashi Kaneko**[a,e,f]

[a] *Theory Center, Institute of Particle and Nuclear Studies, High Energy Accelerator Research Organization (KEK), Tsukuba 305-0801, Japan and School of High Energy Accelerator Science, The Graduate University for Advanced Studies (SOKENDAI), Tsukuba 305-0801, Japan*

[b] *PRISMA+ Cluster of Excellence & Institut für Kernphysik, Johannes-Gutenberg-Universität Mainz, D-55099 Mainz, Germany*

[c] *School of Physics and Astronomy, University of Southampton, Southampton SO17 1BJ, United Kingdom*

[d] *STAG Research Center, University of Southampton, Southampton SO17 1BJ, UK*

[e] *CERN, Theoretical Physics Department, Geneva, Switzerland*

[f] *Kobayashi-Maskawa Institute for the Origin of Particles and the Universe, Nagoya University, Aichi 464–8602, Japan*

E-mail: kelry@post.kek.jp

We report on the calculation of the inclusive semileptonic decay of the D_s meson on the lattice. We simulate the $D_s \to X_s \ell \nu_\ell$ process with Möbius domain-wall charm and strange quarks, whose masses were approximately tuned to the physical values. We cover the whole kinematical region. The focus of this work is on the systematic error due to finite-volume effects. We construct a model of two-body final states to describe the data on a finite volume lattice of $L \simeq 0.055$ fm to investigate the extrapolation to the infinite-volume limit.

The 40th International Symposium on Lattice Field Theory (Lattice 2023)
July 31st - August 4th, 2023
Fermi National Accelerator Laboratory

*Speaker

PoS(LATTICE2023)272

1. Introduction

We update on our work to calculate the inclusive semileptonic decay rate of the D_s-meson. Following our recent work to understand the systematic error associated with the Chebyshev approximation of the kernel function [1], in this paper we report on our estimate of the systematic error due to finite-volume effects. We refer to [1–6] for details on the strategy to calculate inclusive semileptonic decay rates in lattice QCD. In particular, the most recent work [7] presents a comparison between the Chebyshev and Backus-Gilbert approaches to approximate the kernel function in the energy integral.

The rest of this paper is structured as follows. We briefly review the inclusive semileptonic decay on the lattice in Sec. 2. In Sec. 3 we introduce the model used to estimate finite volume effects before applying it to the lattice data in order to extrapolate towards the infinite volume limit in Sec. 4. We present the conclusions in Sec. 5.

2. Inclusive semileptonic decays on the lattice

The total decay rate of the inclusive semileptonic decay is written as

$$\Gamma \sim \int_0^{\boldsymbol{q}^2_{\text{max}}} d\boldsymbol{q}^2 \sqrt{\boldsymbol{q}^2} \sum_{l=0}^{2} \bar{X}^{(l)}(\boldsymbol{q}^2)\,, \tag{1}$$

where $\bar{X}^{(l)}(\boldsymbol{q}^2)$ contains the integral over the hadronic final state energy ω

$$\begin{aligned} \bar{X}^{(l)}_{\sigma}(\boldsymbol{q}^2) &= \int_{\omega_0}^{\infty} d\omega\, W^{\mu\nu}(\boldsymbol{q},\omega) e^{-2\omega t_0} K^{(l)}_{\mu\nu,\sigma}(\boldsymbol{q},\omega) \\ &= \langle \psi^{\mu}(\boldsymbol{q}) | K^{(l)}_{\mu\nu,\sigma}(\boldsymbol{q},\hat{H}) | \psi^{\nu}(\boldsymbol{q}) \rangle\ , \end{aligned} \tag{2}$$

with the hadronic tensor $W^{\mu\nu}(\boldsymbol{q},\omega)$, $|\psi^{\nu}(\boldsymbol{q})\rangle = e^{-\hat{H}t_0}\tilde{J}^{\nu}(\boldsymbol{q},0)\,|D_s\rangle\,/\sqrt{2M_{D_s}}$ and $\tilde{J}^{\nu}(\boldsymbol{q},0)$ being the Fourier transformed currents. The lower limit $0 \le \omega_0 \le \omega_{\text{min}}$ can be chosen freely as there are no states below the lowest lying energy state ω_{min}. The parameter t_0 is introduced to avoid the contact term which receives contributions from the opposite time ordering corresponding to unphysical states. In the definition of $\bar{X}^{(l)}_{\sigma}(\boldsymbol{q}^2)$ above

$$K^{(l)}_{\mu\nu,\sigma}(\boldsymbol{q},\omega) = e^{2\omega t_0}\sqrt{\boldsymbol{q}^2}^{\,2-l}\,(m_{D_s}-\omega)^l \theta_{\sigma}(m_{D_s}-\sqrt{\boldsymbol{q}^2}-\omega)\,, \tag{3}$$

defines the *kernel function* and $\theta_{\sigma}(x)$ is a sigmoid function with smearing width σ.

On the lattice we compute

$$C_{\mu\nu}(t) = \frac{1}{2M_{D_s}} \langle D_s | \tilde{J}^{\mu\dagger}(\boldsymbol{q},0) e^{-\hat{H}t} \tilde{J}^{\nu}(\boldsymbol{q},0) | D_s \rangle\ , \tag{4}$$

and the calculation of the inclusive decay rate is reduced to the one of finding an appropriate polynomial approximation of the kernel function $K^{(l)}_{\mu\nu,\sigma}(\boldsymbol{q},\hat{H})$.

We employ the shifted Chebyshev polynomials $\tilde{T}_j(x)$, with $x = e^{-\omega}$ and define the approximation as

$$\langle K^{(l)}_{\mu\nu,\sigma} \rangle \simeq \frac{1}{2}\tilde{c}^{(l)}_0 \langle \tilde{T}_0 \rangle + \sum_{k=1}^{N} \tilde{c}^{(l)}_k \langle \tilde{T}_k \rangle\ . \tag{5}$$

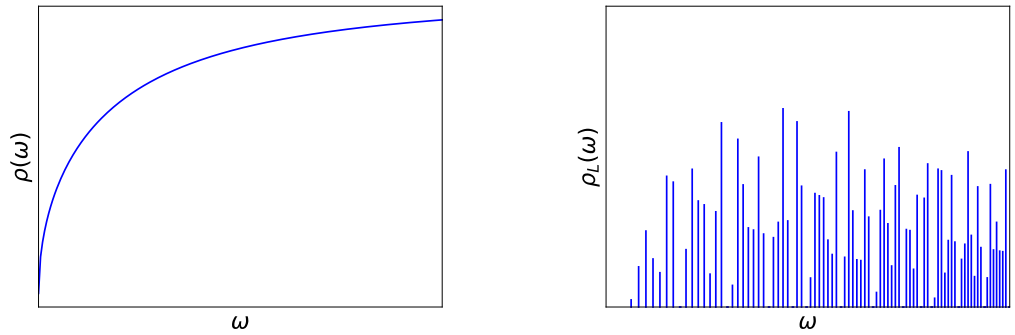

Figure 1: Sketch of the infinite-volume spectral density $\rho(\omega)$ (left) and the finite-volume $\rho_V(\omega)$ for a specific volume V (right). The height of $\rho_V(\omega)$ represents the multiplicity of the states with the same energy ω.

Here, $\tilde{c}_k^{(l)}$ are analytically known coefficients and $\langle \tilde{T}_k \rangle$ are referred to as *Chebyshev matrix elements*. We use the notation $\langle \cdot \rangle \equiv \langle \psi^\mu | \cdot | \psi^\nu \rangle / \langle \psi^\mu | \psi^\nu \rangle$. For simplicity, we skip the indices μ, ν going forward.

The matrix elements are extracted from a fit to the correlator data following

$$\bar{C}(t) = \sum_{j=0}^{t} \tilde{a}_j^{(t)} \langle \tilde{T}_j \rangle \ , \tag{6}$$

where $\tilde{a}_j^{(t)}$ are obtained from the power representation of the Chebyshev polynomials, see (A.24) and (A.25) of [7] for the definition of $\tilde{a}_j^{(t)}$, and $\bar{C}(t)$ is constructed from (4) as $\bar{C}(t) = C(t+2t_0)/C(2t_0)$. To maximize the available data we choose $t_0 = 1/2$. We use priors to ensure that the fitted Chebyshev matrix elements satisfy the condition that the Chebyshev polynomials are bounded, i.e. $\left|\langle \tilde{T}_j \rangle\right| \leq 1$. We refer to [7] for more details on the Chebyshev approximation and the practical application.

3. Modeling strategy

On the lattice, there is a well-known challenge concerning the reconstruction of the spectral density from correlators $C(t)$ with a finite set of discrete time slices, commonly referred to as the ill-posed inverse problem. Even if the inverse problem could be solved for a correlator in a finite volume, $C_V(t)$, where $V = L^3$ denotes the volume of the lattice, and hence the spectral density $\rho_V(\omega)$ is reconstructed, there is still a qualitative difference from its infinite volume counterpart $\rho(\omega)$. The spectral density in the infinite volume is a smooth function, while $\rho_V(\omega)$ is given by a sum of δ-peaks representing allowed states in a finite volume. In Fig. 1 we sketch the situation for two-body states in a finite volume. This problem is avoided by the introduction of the smearing in the kernel function $K(\omega)$ as shown in Eq. (3). The inverse problem is made arbitrarily mild by increasing the smearing width σ, and the smeared spectral density $\rho_{\sigma,V}$ then smoothly approaches its infinite volume counterpart. To recover the inclusive decay rate, we therefore need to take the limit $V \to \infty$ before taking the limit of vanishing smearing width.

The finite-volume effects for the spectral density can be sizeable for multi-body states, because the allowed states are controlled by the boundary condition. The energy spectrum for two-body

states, for instance, receives corrections of $O(1/L^3)$. This would be reduced significantly for the smeared spectral density, but its size and the scaling to the $V \to \infty$ limit may be non-trivial. We therefore introduce a model to investigate the volume dependence. After checking that the model describes the finite-volume data well, we use it to estimate the finite-volume effects.

Among various multi-hadron states, we consider two-body final states, i.e. $K\bar{K}$ states to be specific, which give the dominant contribution. The spectral density is obtained from the imaginary part of the vacuum polarization function, evaluated at one-loop, as

$$\rho(\omega) = \pi \int \frac{d^3\boldsymbol{q}}{(2\pi)^3} \frac{1}{(2\epsilon_{\boldsymbol{q}})^2} \delta(\omega - 2\epsilon_{\boldsymbol{q}}) \tag{7}$$

introducing the short-hand notation $\epsilon_{\boldsymbol{q}}^2 = \boldsymbol{q}^2 + m_K^2$. It corresponds to the production of $K\bar{K}$ states from the vacuum through an operator O, which is taken either as a scalar density ($J = 0$) or vector current ($J = 1$). It models the two-body decays of the D_s meson under an assumption that the wave function of the D_s meson has only insignificant effects, which can be incorporated later by introducing a form factor.

Within this model, one can obtain an explicit expression for the spectral density in the finite-volume and in the infinite-volume limit:

$$\rho_V(\omega) = \frac{\pi}{V} \sum_{\boldsymbol{q}} \frac{1}{4(\boldsymbol{q}^2 + m^2)} \delta\left(\omega - 2\sqrt{\boldsymbol{q}^2 + m^2}\right), \tag{8}$$

and

$$\rho(\omega) = \frac{1}{16\pi} \sqrt{1 - \frac{4m^2}{\omega^2}}, \tag{9}$$

respectively. The expression above corresponds to the scalar density ($J = 0$). For the vector current ($J = 1$), we obtain

$$\rho_V(\omega) = \frac{\pi}{V} \sum_{\boldsymbol{q}} \frac{\boldsymbol{q}^2}{4(\boldsymbol{q}^2 + m^2)} \delta\left(\omega - 2\sqrt{\boldsymbol{q}^2 + m^2}\right). \tag{10}$$

and

$$\rho(\omega) = \frac{1}{64\pi} \omega^2 \left(1 - \frac{4m^2}{\omega^2}\right)^{3/2}, \tag{11}$$

To estimate how the infinite volume limit is approached, we consider

$$\bar{X}^{(l)}(\omega_{\text{th}}) = \int_0^{\omega_{\text{th}}} d\omega \rho(\omega) \times K^{(l)}(\omega), \tag{12}$$

which is defined as a convolution between the kernel and the spectral density. We introduce a variable ω_{th}, which can be understood as a varying energy cut-off in the kernel function. Although ω_{th} is fixed for the physical semileptonic decay process, we use the freedom to choose it in the analysis in order to study how well our model describes the lattice data. In Fig. 2 we show $\bar{X}^{(l)}(\omega_{\text{th}})$ for two choices of the volume $V = 48^3$ and 256^3, as well as the infinite volume limit.

We find that the volume effect depends on the choice of l in the kernel function. As argued in [7], due to the sharp cut around the threshold in the kernel for $l = 0$ (left), a strong dependence on the volume is expected, while $l = 2$ (right) smoothly approaches zero at the threshold and is hence expected to only possesses a mild dependence. Nonetheless, for both cases we observe that $V = 256^3$ nearly reproduces the infinite volume expression.

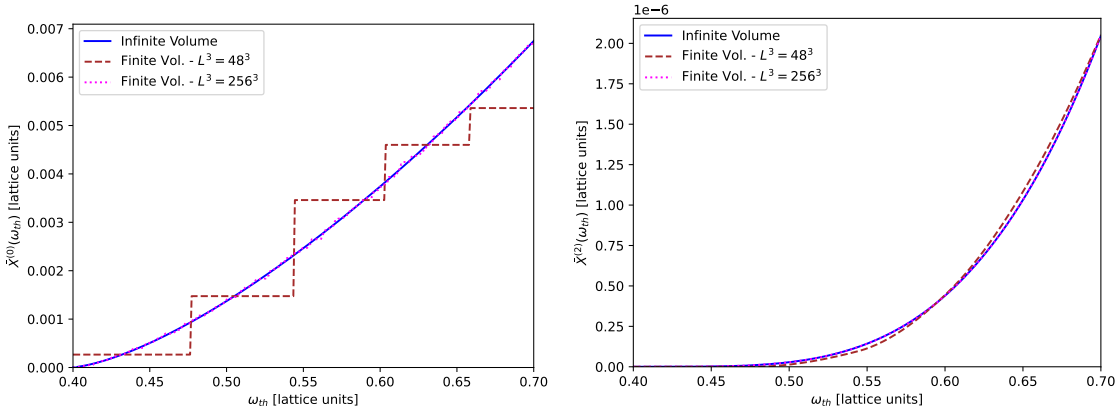

Figure 2: Infinite volume limit (solid line) of the integral (12) and its finite volume evaluation on 48^3 (dashed line) and 256^3 (dash-dotted line) lattices using the finite volume expressions obtained for the spectral density for $J = 0$ with $l = 0$ (left) and $J = 1$ with $l = 2$ (right) as a function of the threshold energy ω_{th}.

4. Systematic error due to finite volume effects

We combine the model and the lattice data to study the infinite volume limit. We construct a fit function of the lattice data

$$\bar{C}(t) = A_0 e^{-E_0 t} + s(L) \sum_i A_i e^{-E_i t} \frac{1}{E_i^2 - m_J^2}\,, \tag{13}$$

where we treat the ground state separately and sum over the two-body excited states in the second term. The factor $1/(E_i^2 - m_J^2)$ appearing in the second term is motivated by the time-like kaon form factor (pole-dominance model) where the mass m_J is that of the state of corresponding quantum number, i.e. f_0 for $J = 0$ and ϕ for $J = 1$. We constrain the prior of the ground state energy E_0 and its amplitude A_0 through a fit to the lattice data. The energies and amplitudes E_i and A_i are taken from our model. The prefactor $s(L)$ is determined by a fit to the lattice data, and thus only the relative magnitude of A_i's are relevant.

We consider the case of the spatial current insertions $A_i A_i$ with vanishing $\boldsymbol{q}^2$. This channel contributes only when $l = 2$ in the kernel function.

In Fig. 3 we compare the fit results to the lattice data of the four-point correlation function. We also include the fit to the ground state. We observe that the short-distance behavior of the correlator, where the excited states contributions become significant, is well described by our fit, while also reproducing the correct long distance behavior.

In Fig. 4 we calculate $\bar{X}^{(l)}(\omega_{\text{th}})$ from (12) using the spectrum determined by the fit. We fit the lattice data at a volume $V = 48^3$ and then use it to calculate results for $V = 256^3$ which serves as a proxy for the infinite volume limit. On the l.h.s. we combine the fit with the kernel function assuming that the cut is implemented through a Heaviside function. On the r.h.s. we show the case assuming a smeared kernel with a smearing width $\sigma = 0.1$. For the latter, we also compare the results with the Chebyshev analysis of the lattice data following (5), where we repeat the analysis for a set of values of ω_{th}. We confirm a good agreement between our model and the results obtained

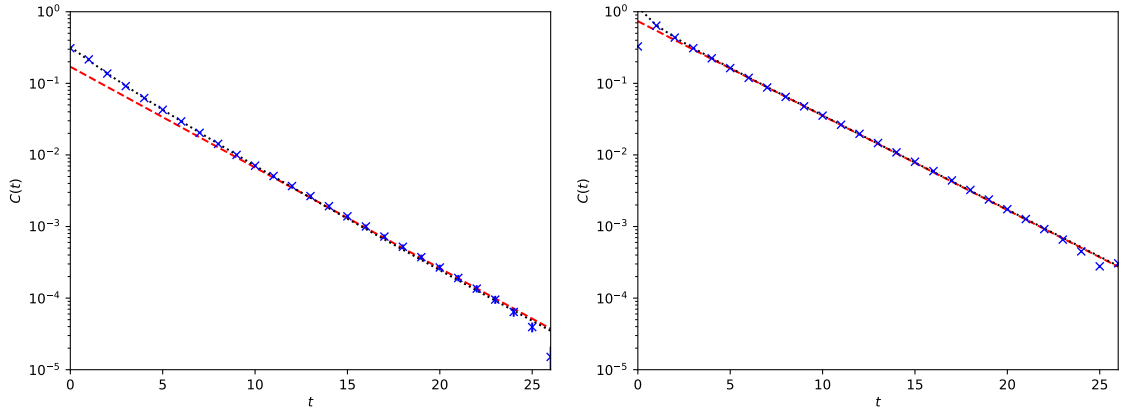

Figure 3: Four-point correlation function for the temporal current insertion of the axial channel (left) and the spatial components (right). For both plots we fit the correlator directly to extract the ground state contribution needed to fix the prior in our model. This fit is represented by the red dashed line. The black dash-dotted line represents the fit results obtained from a fit to our model using the fit prescription (13).

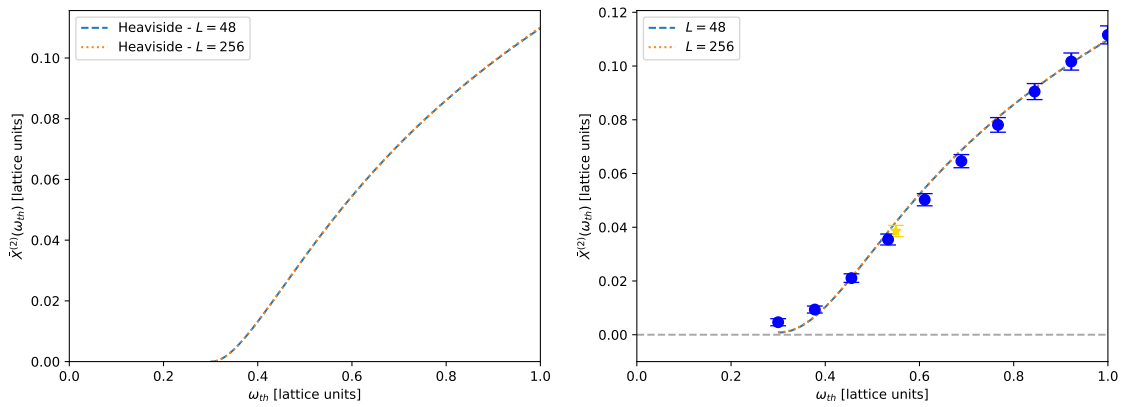

Figure 4: Contribution of spatial currents to $\bar{X}^{\perp,\parallel}_{AA}(\boldsymbol{q}^2)$ at $\boldsymbol{q}^2 = 0\,\text{GeV}^2$. We show the results for two choices of the volume $L = 48^3$ and 256^3. The left panel assumes that the cut-off in the kernel function is implemented through a heaviside function, while the left panel assumes the smeared kernel. For the latter, we also compare the results with those obtained from the Chebyshev analysis of our lattice data evaluated for different choices of the threshold ω_{th} represented by the blue dots. The physical value of the threshold $\omega_{\text{th}} = \omega^{\text{Phys}}_{\text{th}}$ is denoted by the star symbol.

from the lattice data. We conclude that for this specific case the volume dependence is quite mild since no major changes in the shape of the results are found depending on the choice of the volume.

Finally, we address how we construct our estimate of the corrections to the lattice result. The estimate is constructed by adding the corrections from the $V \to \infty$ limit before adding the $\sigma \to 0$ extrapolation, which translates to: $\bar{X}^{\perp}_{AA}(\mathbf{0}^2) = 0.0786(31)$ (lattice result) + $0.0001(0)$ (finite volume correction) $+0.0055(1)$ (Finite smearing correction) $= 0.0843(31)$. For the case considered in this work, the corrections due to the infinite volume limit are negligible, while the $\sigma \to 0$ limit gives a correction of order $\sim 7\,\%$.

5. Conclusion

We developed a model under the assumption of two-body final states for which we have full control over the infinite volume extrapolation and then combine it with a fit to the lattice data to estimate the expected corrections from the infinite volume limit. In the case study performed here we found negligible corrections due to the infinite volume extrapolation, although larger corrections for larger values of $\boldsymbol{q}^2$ and different shapes of the kernel function are expected. Further work is required to give a proper estimate of the systematic error associated with finite volume effects.

Acknowledgments

The numerical calculations of the JLQCD collaboration were performed on SX-Aurora TSUBASA at the High Energy Accelerator Research Organization (KEK) under its Particle, Nuclear and Astrophysics Simulation Program, as well as on Fugaku through the HPCI System Research Project (Project ID: hp220056).

The works of S.H. and T.K. are supported in part by JSPS KAKENHI Grant Numbers 22H00138 and 21H01085, respectively, and by the Post-K and Fugaku supercomputer project through the Joint Institute for Computational Fundamental Science (JICFuS).

References

[1] R. Kellermann, A. Barone, S. Hashimoto, A. Jüttner and T. Kaneko, PoS **LATTICE2022**, 414 (2023) doi:10.22323/1.430.0414 [arXiv:2211.16830 [hep-lat]].

[2] P. Gambino and S. Hashimoto, Phys. Rev. Lett. **125** (2020) no.3, 032001 doi:10.1103/PhysRevLett.125.032001 [arXiv:2005.13730 [hep-lat]].

[3] P. Gambino, S. Hashimoto, S. Mächler, M. Panero, F. Sanfilippo, S. Simula, A. Smecca and N. Tantalo, JHEP **07** (2022), 083 doi:10.1007/JHEP07(2022)083 [arXiv:2203.11762 [hep-lat]].

[4] M. T. Hansen, H. B. Meyer and D. Robaina, Phys. Rev. D **96** (2017) no.9, 094513 doi:10.1103/PhysRevD.96.094513 [arXiv:1704.08993 [hep-lat]].

[5] M. Hansen, A. Lupo and N. Tantalo, Phys. Rev. D **99** (2019) no.9, 094508 doi:10.1103/PhysRevD.99.094508 [arXiv:1903.06476 [hep-lat]].

[6] J. Bulava, M. T. Hansen, M. W. Hansen, A. Patella and N. Tantalo, JHEP **07** (2022), 034 doi:10.1007/JHEP07(2022)034 [arXiv:2111.12774 [hep-lat]].

[7] A. Barone, S. Hashimoto, A. Jüttner, T. Kaneko and R. Kellermann, JHEP **07**, 145 (2023) doi:10.1007/JHEP07(2023)145 [arXiv:2305.14092 [hep-lat]].